Tangential large scale structure as a standard ruler: curvature parameters from quasars

B. F. Roukema, G. A. Mamon

Astron. Astrophys. 358, 395–408 (2000)

ASTRONOMY AND ASTROPHYSICS

Tangential large scale structure as a standard ruler: curvature parameters from quasars

B.F. Roukema[1] **and G.A. Mamon**[2,3]

[1] Inter-University Centre for Astronomy and Astrophysics, Post Bag 4, Ganeshkhind, Pune, 411 007, India (boud@iucaa.ernet.in)
[2] Institut d'Astrophysique de Paris (CNRS UPR 341), 98bis Bd Arago, 75014 Paris, France (gam@iap.fr)
[3] DAEC (CNRS UMR 8631), Observatoire de Paris-Meudon, 5 place Jules Janssen, 92195 Meudon Cedex, France

Received 22 November 1999 / Accepted 17 April 2000

Abstract. Several observational analyses suggest that matter is spatially structured at a scale of $L_{\rm LSS} \approx 130\,h^{-1}$ Mpc at low redshifts. This peak in the power spectrum provides *a standard ruler in comoving space* which can be used to compare the local geometry at high and low redshifts, thereby constraining the curvature parameters.

It is shown here that this power spectrum peak is present in the observed quasar distribution at $z \sim 2$: qualitatively, via wedge diagrams which clearly show a void-like structure, and quantitatively, via one-dimensional Fourier analysis of the quasars' tangential distribution. The sample studied here contains 812 quasars.

The method produces strong constraints (68% confidence limits) on the density parameter Ω_0 and weaker constraints on the cosmological constant λ_0, which can be expressed by the relation $\Omega_0 = (0.24 \pm 0.15) + (0.10 \pm 0.08)\,\lambda_0$. Independently of λ_0 (in the range $\lambda_0 \in [0,1]$), the constraint is $0.1 < \Omega_0 < 0.45$. Constraints if the cosmological constant is zero or if $\lambda_0 \equiv 1 - \Omega_0$ are $\Omega_0 = 0.24^{+0.05}_{-0.15}$ and $\Omega_0 = 0.30 \pm 0.15$ respectively.

The power spectrum peak method is independent from the supernovae Type Ia method by choice of astrophysical object, by redshift range, and by use of a standard ruler instead of a standard candle. Combination of the two results yields $\Omega_0 = (0.30 \pm 0.11) + (0.57 \pm 0.11)(\lambda_0 - 0.7)$, $0.55 < \lambda_0 < 0.95$, (68% confidence limits) *without assuming that* $\lambda_0 \equiv 1 - \Omega_0$. This strongly supports the possibility that the observable universe satisfies a nearly flat, perturbed Friedmann-Lemaître-Robertson-Walker model, *independently of any cosmic microwave background observations*.

In other words it has been shown that $\Omega_0 + \lambda_0 = (1.0 \pm 0.11) + (1.57 \pm 0.11)(\lambda_0 - 0.7)$.

Key words: cosmology: observations – cosmology: theory – galaxies: quasars: general – cosmology: distance scale – cosmology: large-scale structure of Universe – reference systems

1. Introduction

It has been known for more than a decade (e.g. de Lapparent et al. 1986; Geller & Huchra 1989) that the spatial distribution of extragalactic objects is structured at length scales about an order of magnitude greater than the $r_0 \approx 5\,h^{-1}$ Mpc scale which characterises galaxy clustering via the two-point auto-correlation function. Observational analyses from several different data sets suggest that this is due to a characteristic length scale at $L_{\rm LSS} \approx 130\,h^{-1}$ Mpc, or in other words, that there is a maximum in the power spectrum at $k = 2\pi/L_{\rm LSS} \approx 0.05\,h\,{\rm Mpc}^{-1}$ (e.g. Broadhurst et al. 1990; Broadhurst 1999; Broadhurst & Jaffe 1999; da Costa 1992; da Costa et al. 1993; Baugh & Efstathiou 1993, 1994; Gaztañaga & Baugh 1998; Einasto et al. 1994, 1997a,b; Deng et al. 1996 or Guzzo 1999 for a recent review).

It has already been suggested that this scale could be used as a standard ruler which could be compared at low and high redshifts in order to constrain the curvature parameters, Ω_0 (the density parameter) and λ_0 (the dimensionless cosmological constant). In the redshift direction, at least two analyses have been carried out based on this idea: one analysis of a quasar catalogue and one analysis of Lyman break galaxies.

Deng et al. (1994) implicitly used the large scale structure scale as a curvature constraint in quasar data, under the assumption that $\lambda_0 \equiv 0$, and found that $\Omega_0 \approx 0.4$. Broadhurst & Jaffe used the radial (redshift) distribution of Lyman break galaxies at $z \sim 3$ (Table 1, Giavalisco et al. 1998; Fig. 2, Adelberger et al. 1998). They found a correlation scale of $\Delta z \approx 0.22 \pm 0.02$, and inferred a relation $3.2\,\Omega_0 - \lambda_0 \approx 0.7$.

The purpose of this paper is to (i) emphasise that the principle can be applied to a class of bright objects easily found at super-unity redshifts: quasars; (ii) show that redshift selection effects can be minimised by using the tangential distribution instead of the radial distribution; and (iii) show pictorially (i.e. qualitatively) that quasars do indeed trace large scale structure at $z \sim 2$.

(i) Because quasars are much brighter than Lyman break galaxies, they offer a potentially much more rapid method of obtaining high precision estimates of the curvature parameters than the latter. Both classes of objects have the advantage relative to supernovae type Ia (Perlmutter et al. 1999; Riess et al. 1998) of being at super-unity redshifts, so that the dependence on the curvature parameters is strong.

(ii) In order to avoid the well-known selection effects in the redshift distribution of quasars (which could also in principle

Send offprint requests to: B.F. Roukema

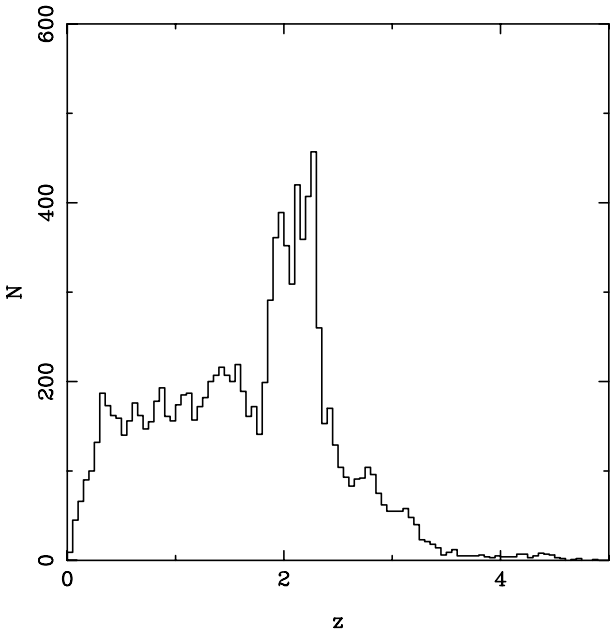

Fig. 1. Redshift distribution of quasars in the compilation of Véron-Cetty & Véron (1998).

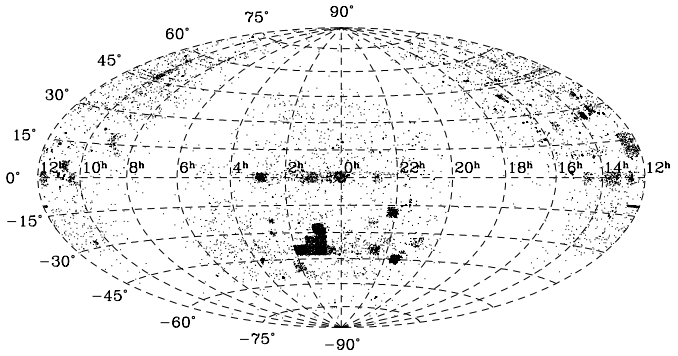

Fig. 2. Sky distribution of quasars in the compilation of Véron-Cetty & Véron (1998).

affect the redshift distribution of Lyman break galaxies), the *tangential* distance distribution of quasars is investigated.

(iii) However, two-dimensional wedge diagrams are also plotted to show clear qualitative evidence of the tracing of large scale structure by the quasar distribution.

Details of the method and selection of homogeneous quasar samples are described in Sect. 2. Results are presented in Sect. 3, and discussion and conclusions are presented in Sect. 4.

A perturbed Friedmann-Lemaître-Robertson-Walker cosmological model is assumed here. The context in which quasars could reasonably be expected to form a tracer population of large scale structure may be any model in which quasars form in galaxy centres or in which galaxies form around quasars. The expected short life times of quasars should not prevent them from forming a tracer population, though they might form a biased population which could either weaken or strengthen the amplitude of the signal.

The Hubble constant is parametrised here as $h \equiv H_0/100\,\mathrm{km\ s^{-1}\ Mpc^{-1}}$. Comoving coordinates are used throughout [i.e. 'proper distances', eq. (14.2.21), Weinberg (1972), equivalent to 'conformal time' if $c = 1$]. Values of the density parameter, Ω_0, and the dimensionless cosmological constant, λ_0, are indicated where used.

2. Method

2.1. Choice of catalogue and sky regions

There are now around 10^4 quasars which have publicly available redshifts and celestial positions (Véron-Cetty & Véron 1998). What is the optimal way to search for the power spectrum peak among these data?

Figs. 1 and 2 show the redshift and sky distributions of these quasars. Depending on the redshift range of any quasar sample, a few hundred h^{-1} Mpc typically correspond to $\Delta z \sim 10^{-1}$ in redshift to within an order of magnitude, and at $z \sim 2$, where the peak in the redshift distribution lies, to $\Delta\theta \sim 1°$.

There is clearly structure in the combined redshift histogram for the full sky at around this scale. As discussed in detail by Scott (1991), the ratios in wavelength of important emission lines which contribute to the chance of detecting a quasar (Lyα, C IV, C III, Mg II) correspond to intervals $\Delta \ln \lambda \approx 0.2$ and clearly contribute to the obvious peaks in the distribution.

The alternative to searching for structure in the redshift direction is to search in the tangential direction. Most of the deep surveys visible in Fig. 2 are based on photometric selection from photographic plates of size roughly $6° \times 6°$, in particular from objective prism surveys. This is moderately larger than the scale of interest.

In order to minimise possible systematic effects due to obscuration by dust and modification of the sky background by bright stars, surveys near the South or North galactic poles would be best.

Near the South galactic pole (SGP), several regions have been observed contiguously, with (at least to the eye) a reasonable homogeneity across the different plates in the region.

More objectively, the largest single homogeneous subset of the Véron-Cetty & Véron (1998) catalogue in the SGP region is that of Iovino et al. (1996), who used an 'automatic quasar detection' method, i.e. applied a computer algorithm to the digitised images of objective prism plates taken on the UK Schmidt Telescope at Siding Spring, Australia.

This is the catalogue chosen for analysis here. The overall redshift distribution of this catalogue is shown in Fig. 3, and the sky distribution of the $1.8 \leq z < 2.4$ component is shown in Fig. 4.

Wedge diagrams of the catalogue, within the limits of Table 1 (see Sect. 2.2) are shown in Fig. 5. Note that the right ascension and declination subsamples are not entirely independent sets of quasars (see Fig. 4), though since only one angular coordinate is used in each analysis, they are very close to being effectively independent. Although quantitative analysis in these planes would be difficult to carry out due to the obvious

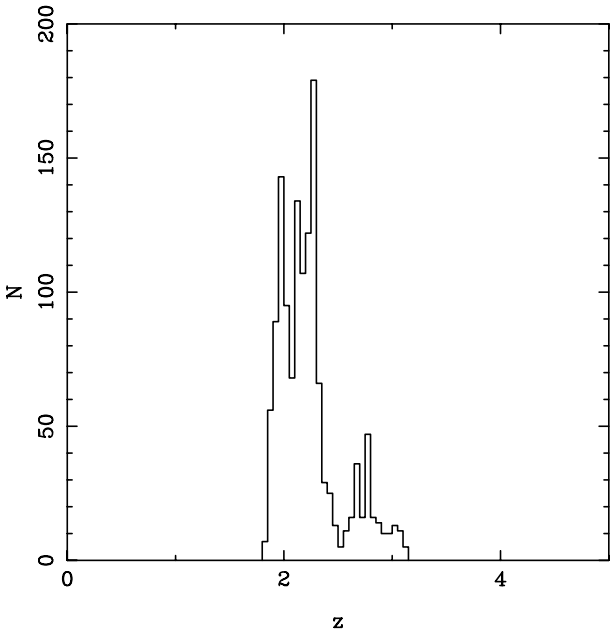

Fig. 3. Redshift distribution of quasars with redshifts from Iovino et al. (1996).

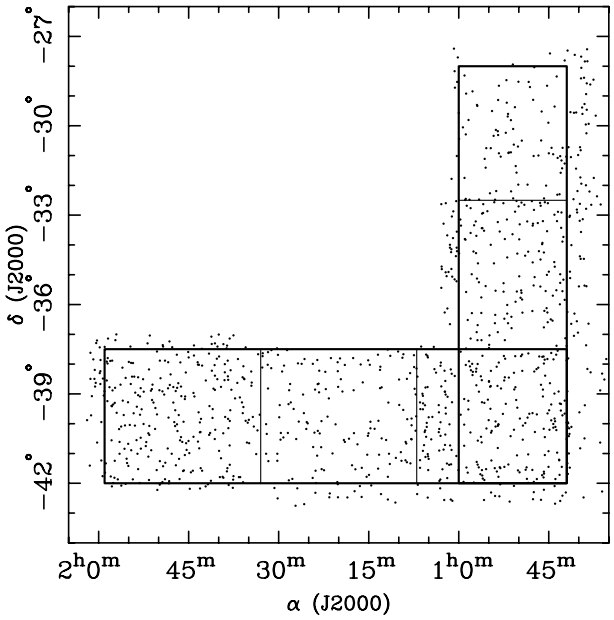

Fig. 4. Sky distribution of quasars with redshifts from Iovino et al. (1996), which lie in the redshift range $1.8 \leq z < 2.4$. Thick lines show the outlines of the right ascension and declination samples chosen for one-dimensional Fourier analysis. Thin vertical and horizontal lines show divisions in right ascension and declination in the right ascension and declination subsamples respectively, which simulated distributions are Poisson distributed. See Table 1 for numerical values of these limits.

redshift selection effects, it is qualitatively clear that a void-like structure is present, at a scale near $L_{\rm LSS} \sim 130\,h^{-1}$ Mpc for $(\Omega_0 = 0.3, \lambda_0 = 0.7)$. In order to avoid the redshift selection effects (see also Hartwick & Schade 1990; Scott 1991), the analysis here is restricted to Fourier space.

Table 1. Definition of the two tangentially long, densely observed, homogeneous, subsamples of the Iovino et al. (1996) quasar survey listed in the Véron-Cetty & Véron (1998) catalogue, near the south galactic pole (SGP). The right ascension (first row) and declination (second row) subsamples are defined by J2000 limits ($\alpha_1 \leq \alpha \leq \alpha_2$, $\delta_1 \leq \delta \leq \delta_2$). For the purpose of Poisson simulations, these are subdivided in right ascension at (α', α'') and in declination at (δ', δ''), in order to allow for the possibility of different magnitude zero points or different magnitude cutoffs in the different plates. The number of objects N in each subsample is indicated. The total number of physically distinct quasars in the two subsamples is $N_{\rm tot} = 812$.

α_1	α_2	δ_1	δ_2	α'	α''	δ'	δ''	N
'Right ascension (α) subsample'								
0^h42^m	1^h59^m	-42.0	-37.5	1^h07^m	1^h33^m			604
'Declination (δ) subsample'								
0^h42^m	1^h00^m	-42.0	-28.0			-37.5	-32.5	373

2.2. One-dimensional Fourier analysis

The study of structure at $L_{\rm LSS}$ is made by one-dimensional Fourier analysis of two subsamples of the Iovino et al. (1996) sample [i.e. of the subset of the Véron-Cetty & Véron catalogue for which redshifts are obtained from Iovino et al. (1996)] which have maximum tangential survey length. That is, one subsample combining three plates in the right ascension direction and one subsample combining three plates in the declination direction are chosen.

The right ascension and declination boundaries are chosen conservatively, i.e. to within at most 2.5 great circle degrees from the plate centres, and are shifted even closer in where it looks like there may be incompleteness close to the boundary. Although what appears to be a lack of quasars near a few plate boundaries might in fact be due to real voids, it is preferable to risk losing some real signal rather than risk including some noise.

The angular limits chosen are indicated in Table 1. The redshift range used is $z_1 = 1.8 \leq z < z_2 = 2.4$, which includes most of the catalogue, and is small enough to superimpose only a few 'units' of large scale structure, i.e. the signal should not be significantly reduced by the superimposition of structures which are out of phase.

In each of the two subsamples, the angular positions in the long direction (right ascension and declination respectively) are converted to comoving tangential lengths $d_\perp$ by

$$d_\perp(z,\theta) \equiv (\theta - \theta_1)\, d_{\rm pm}(z) = (\theta - \theta_1) \begin{cases} R_C \sinh[d(z)/R_C], & \kappa_0 < 0 \\ d(z), & \kappa_0 = 0 \\ R_C \sin[d(z)/R_C], & \kappa_0 > 0. \end{cases} , \quad (1)$$

where the angular position $\theta = \alpha \cos\delta$ or $\theta = \delta$ and the survey limit is $\theta_1 = \alpha_1 \cos\delta_1$ or $\theta_1 = \delta_1$ respectively (in radians), $d_{\rm pm}(z)$ is the proper motion distance,

$$d(z) = \frac{c}{H_0} \int_{1/(1+z)}^{1} \frac{{\rm d}a}{a\sqrt{\Omega_0/a - \kappa_0 + \lambda_0 a^2}}, \quad (2)$$

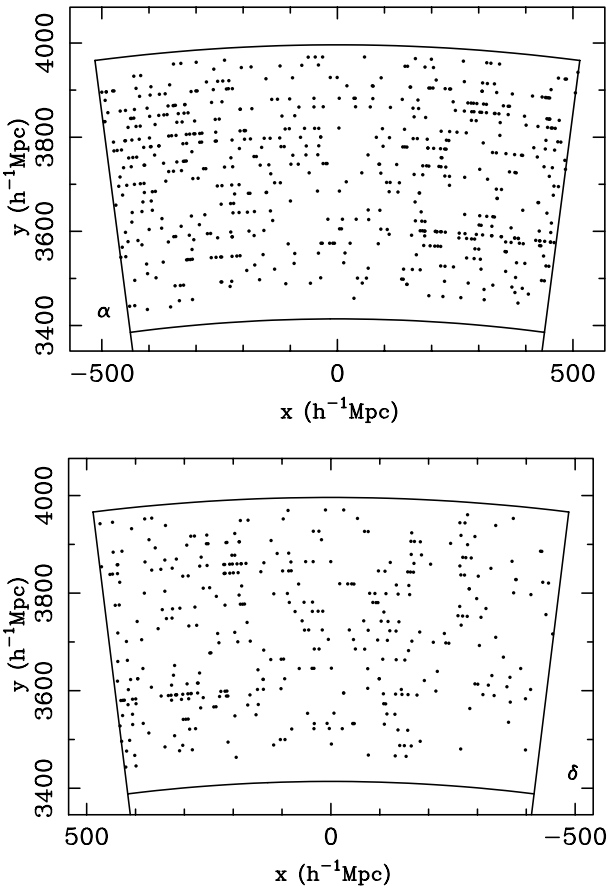

Fig. 5. Wedge diagrams for the for the right ascension (upper panel) and declination (lower panel) subsamples, for $(\Omega_0 = 0.3, \lambda_0 = 0.7)$. Since curvature is zero, rectlinear coordinates are defined: $x = d_{\rm pm}\cos(\theta^* - \theta), y = d_{\rm pm}\sin(\theta^* - \theta)$, where $\theta^* \equiv (\theta_1 + \theta_2)/2 + \pi/2$ and $\theta, \theta_1, \theta_2$ and $d_{\rm pm}$ are defined in Sect. 2.2. Voids consistent with $L_{\rm LSS} = 130 \pm 10\,h^{-1}$ Mpc and not due to selection effects are clearly visible.

is the proper distance [eq. (14.2.21), Weinberg (1972)],

$$\kappa_0 \equiv \Omega_0 + \lambda_0 - 1 \tag{3}$$

is the (dimensionless) curvature of the observational Universe and

$$R_C \equiv \frac{c}{H_0}\frac{1}{\sqrt{|\kappa_0|}} \tag{4}$$

is its curvature radius.

The maximum tangential length considered is $d_\perp(z_1, \theta_2)$, where $z_1 = 1.8$ is the low redshift limit of the sample. This is the minimum tangential length corresponding to $\theta_2 - \theta_1$ over the range in z and the (Ω_0, λ_0) domain considered in this paper. For negative or zero curvature, $d_\perp$ is always an increasing function of z. For positive curvature and $\Omega_0 < 1.1, \lambda_0 < 1$, the $d/R_C = \pi/2$ point (halfway to the antipode) occurs at $z \gtrsim 8$, so the domain of decreasing $d_\perp$ is not reached here. Thus, $d_\perp$ is a strictly increasing function of z in the domain of interest of this paper and $d_\perp(z_1)$ provides the minimum tangential length.

Note that the choice of this cutoff throws away a small amount of data (e.g. for which $z \approx z_2, \theta \approx \theta_2$), but ensures that the one-dimensional number density distribution $\mathrm{d}N/\mathrm{d}d_\perp$ is a uniform projection of a (large) subset of the two-dimensional distribution $\mathrm{d}^2N/\mathrm{d}d_\perp \mathrm{d}d_{\rm pm}$. Inclusion of the small amount of lost data would create a nonuniform number density projection and would introduce non-physical power to the Fourier transform, so is not attempted here.

For values of (Ω_0, λ_0) in the range $0.0 \le \Omega_0 \le 1.1, -0.1 \le \lambda_0 \le 1.0$, the list of positions $0 \le d_\perp \le d_\perp(z_1, \theta_2)$ is binned into 1024 bins and fast Fourier transformed to a function $f(\nu|\Omega_0, \lambda_0)$. The results below are found to change slightly but insignificantly if fewer bins, e.g. 128 bins, are used. The contours in the (Ω_0, λ_0) plane are more noisy with fewer bins.

Two null hypotheses are considered here for the Fourier spectrum for each pair (Ω_0, λ_0): the possibility that large scale structure is undetectable in the two quasar subsamples, and the possibility that the best estimate of the scale of large scale structure is $L_{\rm LSS} \pm \Delta L_{\rm LSS}$.

2.3. Null hypothesis $\mathcal{H}_1$: no LSS peak is detectable

Informally, $\mathcal{H}_1(\Omega_0, \lambda_0)$ is the hypothesis that there is no peak in the tangential distributions of the quasars due to large scale structure.

More precisely, $\mathcal{H}_1(\Omega_0, \lambda_0)$ is the hypothesis that:

(i) the pair (Ω_0, λ_0) is correct;
(ii) the value of the Fourier transform f at the large scale structure frequency $\nu_0 \equiv 1/L_{\rm LSS}$, i.e. $f(\nu_0|\Omega_0, \lambda_0)$, is not significantly higher than that expected from the distribution of the same statistic evaluated for Poisson distributions in θ, for fixed values of $\nu_0, \Omega_0, \lambda_0$, for both subsamples; and
(iii) $\nu_{\rm max}$, defined as the local maximum in $f(\nu|\Omega_0, \lambda_0)$ at the greatest value of ν satisfying $\nu < 0.01\,h\,\mathrm{Mpc}^{-1}$, is not significantly higher than that expected from the distribution of the same statistic evaluated for Poisson distributions in θ, for fixed values of Ω_0, λ_0, for both subsamples.

The Poisson distributions are pseudo-random samplings of uniform distributions in θ within each of the three subdivisions of the sample as defined as in Table 1. The number of simulations calculated is 30. A Gaussian smoothing of standard deviation two bin widths is applied to the Fourier transform $f(\nu|\Omega_0, \lambda_0)$ before searching for the local maximum.

The purpose of criterion (ii) is that if a peak is present at the scale expected, then this may contribute to rejecting $\mathcal{H}_1$ by the presence of a strong peak. However, because the overdensity may not be very high, this may not be sufficient in itself to reject $\mathcal{H}_1$.

An independent and possibly more sensitive test is (iii): is the best estimate of the frequency of a peak significantly different from that for Poisson distributions, independently of any criterion on the absolute height of the peak? Likely values of $\langle\nu_{\rm max}\rangle$ for Poisson simulations are around $0.005\,h\,\mathrm{Mpc}^{-1}$, though this depends on the smoothness or roughness of f for the Poisson simulations. Since $1/L_{\rm LSS} \approx 0.0077\,h\,\mathrm{Mpc}^{-1}$, then, as long as the scatter in $\nu_{\rm max}$ for the simulations is small enough, criterion (iii) may enable rejection of $\mathcal{H}_1$ for pairs (Ω_0, λ_0) which

correctly describe the observational Universe, because in that case (under the principle assumed for this paper), the peak is expected to occur at a special frequency rather than at an arbitrary frequency.

2.4. Null hypothesis $\mathcal{H}_2$: the best estimate of the frequency of an LSS peak is at $1/L_{\rm LSS}$

The more interesting hypothesis is $\mathcal{H}_2(\Omega_0, \lambda_0)$, the hypothesis that the best estimate of a peak in the tangential distributions of the quasars due to large scale structure is at $L_{\rm LSS} \pm \Delta L_{\rm LSS}$, independently of whether the peak is significant or not.

$\mathcal{H}_2(\Omega_0, \lambda_0)$ is quantified as follows:

(i) the pair (Ω_0, λ_0) is correct;
(ii) $\nu_{\rm max}$ (defined as for $\mathcal{H}_1$) is consistent with $\nu_{\rm max} = 1/L_{\rm LSS}$ where the $1\,\sigma$ uncertainty in the external estimate of $L_{\rm LSS}$ is $\Delta L_{\rm LSS}$, and $\Delta\nu_{\rm max}$, the $1\,\sigma$ uncertainty in estimating $\nu_{\rm max}$ from the present data is obtained robustly by bootstraps (e.g. Barrow et al. 1984).

The estimate $\Delta L_{\rm LSS} = 10\,h^{-1}$ Mpc is adopted here.

The bootstrap method (e.g. Barrow et al. 1984) for a catalogue of N objects, is for N objects to be randomly drawn from the same sample, *allowing multiple sampling* of single objects. The statistical uncertainties in the properties of interest are then estimated by running several such bootstrap simulations, which are considered as independent experiments. This provides an upper estimate to the uncertainty. The number of bootstraps used here is 30.

The bootstrap $1\,\sigma$ uncertainty and $\Delta L_{\rm LSS}$ are assumed to be independent and to arise from Gaussian distributions, so are combined in quadrature.

Although $\mathcal{H}_2$ could in principle be consistent with the data for (Ω_0, λ_0) pairs which are also consistent with $\mathcal{H}_1$, the (Ω_0, λ_0) pairs for which $\mathcal{H}_1$ is rejected and $\mathcal{H}_2$ is not rejected are obviously of most interest.

3. Results

3.1. $\mathcal{H}_1$: can the absence of a peak be rejected?

Confidence levels $1 - P_\alpha[f(\nu_0)], 1 - P_\alpha(\nu_{\rm max}), 1 - P_\delta[f(\nu_0)]$ and $1 - P_\delta(\nu_{\rm max})$, for rejecting $\mathcal{H}_1$ are shown in Figs. 6 and 7 for the right ascension and declination subsamples respectively.

These are defined by the probability of the observational results given the hypothesis:

$$P(t) \equiv P_{\rm gauss}(t, \bar{t}, \Delta t) \equiv \int_{|t-\bar{t}|/\Delta t}^{\infty} \frac{1}{\sqrt{2\pi}} e^{-u^2/2}\, du, = \frac{1}{2}{\rm erfc}\left(\frac{1}{\sqrt{2}}\frac{|t-\bar{t}|}{\Delta t}\right) \quad (5)$$

where t is the parameter studied (either $f(\nu_0)$ or $\nu_{\rm max}$), and $\bar{t}$ and Δt are the mean value of t and the standard deviation of t obtained from the Poisson simulations.

Since the question of interest is to find (Ω_0, λ_0) pairs for which there is, ideally, an excess of power at $L_{\rm LSS}$ and a frequency higher than that for Poisson distributions (given the limits for searching for a local maximum defined in Sect. 2.3), the probability above is defined to be one-sided.

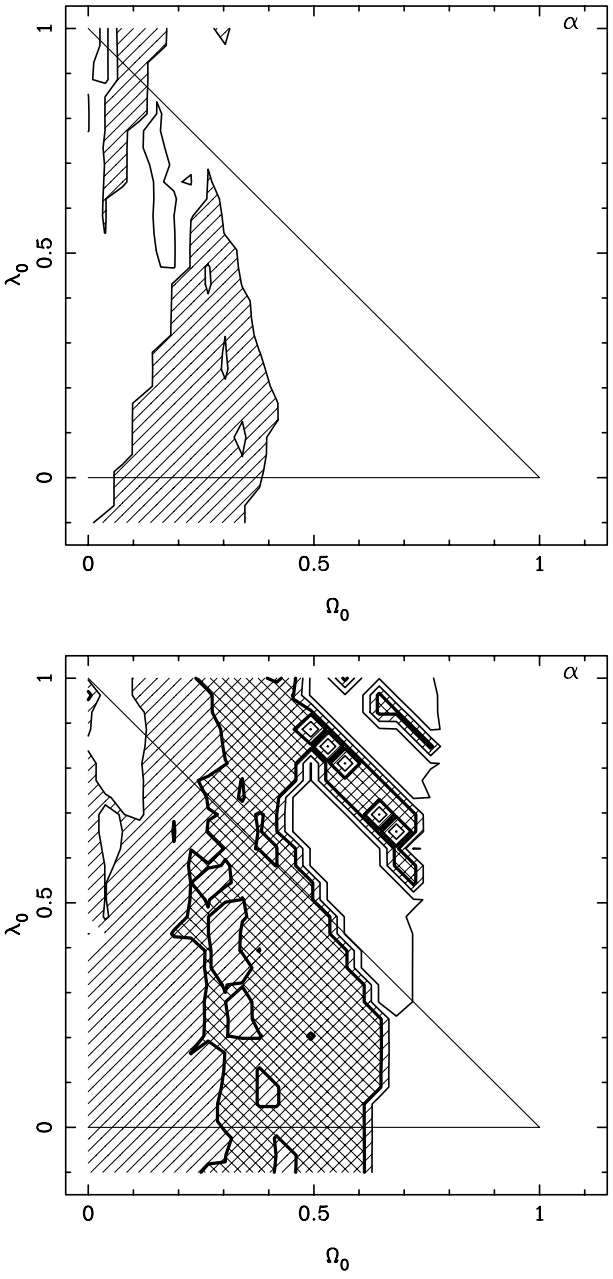

Fig. 6. Confidence levels for the different criteria for trying to reject $\mathcal{H}_1$, for the right ascension subsample. The upper panel is for $f(\nu_0)$, the lower panel for $\nu_{\rm max}$. Rejection of the null hypothesis $\mathcal{H}_1$ at $> 0\,\sigma$, $> 1\,\sigma$, $> 2\,\sigma$ and $> 3\,\sigma$ confidence levels, i.e. $1-P > 50\%, 1-P > 84\%$, $1 - P > 98\%$ and $1 - P > 99.9\%$, is shown by contoured regions with light shading, light cross-hatched, medium cross-hatched and heavy cross-hatched shading, respectively. (In a few of this set of figures, a few contours at $< 0\,\sigma$ and $< -1\,\sigma$ are also shown. These are not useful for null hypothesis rejection.) Lines indicating $\lambda_0 = 0$ and $\lambda_0 = 1 - \Omega_0$ are shown for $\Omega_0 \leq 1$ as a guide to the eye.

The upper panel of Fig. 6 shows that if there is a peak at $L_{\rm LSS}$ in the right ascension subsample, then it is not strong enough to

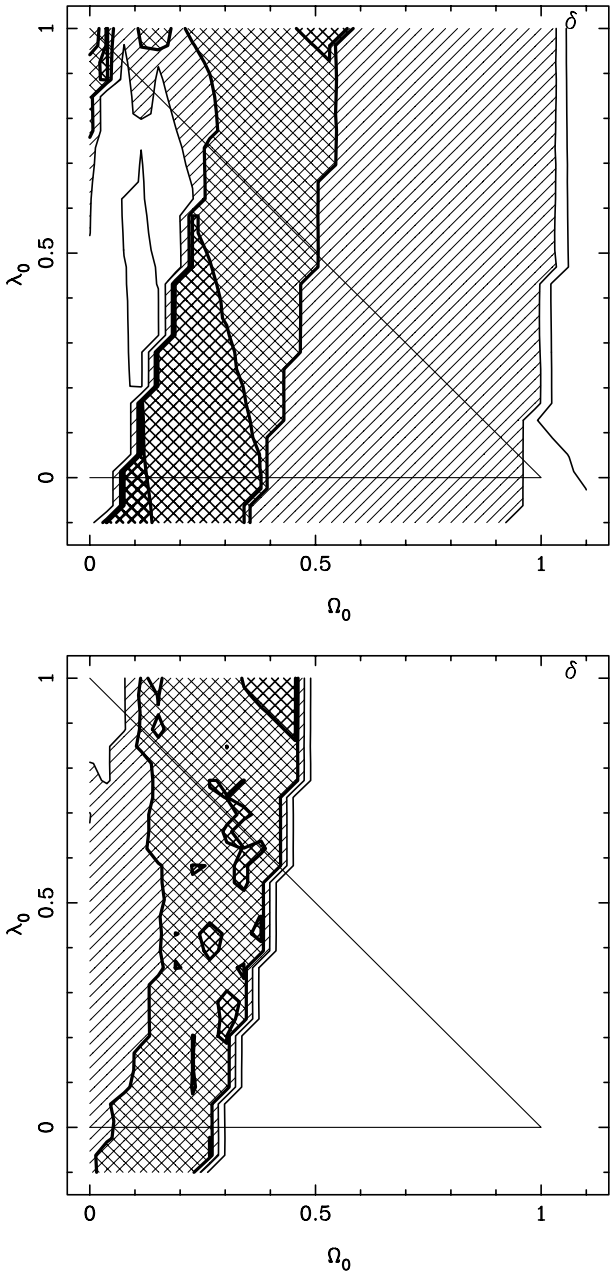

Fig. 7. Confidence levels for rejecting $\mathcal{H}_1$, for the declination subsample. The upper panel is for $f(\nu_0)$, the lower panel for $\nu_{\max}$. Shading is as for Fig. 6.

significantly reject the null hypothesis $\mathcal{H}_1(\Omega_0, \lambda_0)$ of the non-existence of a peak for any pair (Ω_0, λ_0). Note, of course, that non-rejection of $\mathcal{H}_1$ does not imply that $\mathcal{H}_1$ is correct. It just implies (states) that $\mathcal{H}_1$ is not rejected.

However, the lower panel of Fig. 6 shows that the best estimate of the frequency of a peak, independently of its significance, *is* rejected at the $1 - P > 84\%$ level for a large (though noisy) band in the (Ω_0, λ_0) plane, for $\Omega_0 \sim 0.4 \pm 0.1$.

Both the $f(\nu_0)$ amplitude test and the $\nu_{\max}$ test for the declination subsample (Fig. 7) independently confirm, to $\sim \pm 0.2$ precision in Ω_0 and λ_0, the region of the (Ω_0, λ_0) plane which enables $1\,\sigma$ rejection of $\mathcal{H}_1(\Omega_0, \lambda_0)$. A small band within the latter, for the $\nu_{\max}$ test, enables rejection to $2\,\sigma$, i.e. $1 - P > 98\%$.

As noted above, the fact that the $f(\nu_0)$ test for the right ascension sample does not reject $\mathcal{H}_1$ is not a problem for alternative hypotheses to $\mathcal{H}_1$ (in particular for $\mathcal{H}_2$). The failure of one test to reject a model does not imply that it is correct, and in the presence of independent tests which *do* reject the model, the overall result should be to reject the model. This is expressed mathematically as follows.

The results for the two tests, for the two subsamples, imply a confidence level

$$1 - P = 1 - \; P_\alpha[f(\nu_0)] \;\; P_\alpha[\nu_{\max}] \;\; P_\delta[f(\nu_0)] \;\; P_\delta[\nu_{\max}] \quad (6)$$

for rejecting $\mathcal{H}_1$. Note that although the $f(\nu_0)$ and $\nu_{\max}$ tests seem to be independent (e.g. Figs. 6, 7), this has not been strictly proven, so the combined confidence levels for rejecting $\mathcal{H}_1$ may be slightly overestimated.

The final contours in confidence levels for rejecting $\mathcal{H}_1(\Omega_0, \lambda_0)$ are shown in Fig. 8.

These show that the null hypothesis of the absence of the large scale structure peak is rejected at at least the $1 - P > 84\%$ level for nearly all pairs (Ω_0, λ_0) with $0 \lesssim \Omega_0 \lesssim 0.6$ and at the $1 - P > 98\%$ level for $0.1 \lesssim \Omega_0 \lesssim 0.5$. Moreover, for a band running from $(\Omega_0 \approx 0.15, \lambda_0 = -0.1)$ to $(\Omega_0 \approx 0.4, \lambda_0 = 1)$, $\mathcal{H}_1(\Omega_0, \lambda_0)$ is rejected at the $1 - P > 99.9\%$ level.

In other words, if the matter density of the Universe is low, then the possibility that there is no large scale structure peak at $L_{\rm LSS} = 130\,h^{-1}$ Mpc in the quasar sample is rejected, and it is rejected to high significance for the most favoured values of the (Ω_0, λ_0) pair: a low density hyperbolic model with $(\Omega_0 \approx 0.2, \lambda_0 = 0)$, or a low density flat model with $(\Omega_0 \approx 0.3, \lambda_0 = 1 - \Omega_0)$.

For a flat, critical density model, $(\Omega_0 = 1, \lambda_0 = 0)$, $\mathcal{H}_1$ is not rejected. Could it be argued that if $(\Omega_0 = 1, \lambda_0 = 0)$ is correct, then the rejection of $\mathcal{H}_1$ for low values of Ω_0 is simply an artefact due to making a wrong assumption?

A simple, quantified counterargument to this is the following. If a peak really is present in the data, even though its amplitude may be low, then even for incorrect values of (Ω_0, λ_0) it is likely that non-random frequencies can be detected. Since the search for the frequency starts just a little above $1/L_{\rm LSS}$, then if a low value of Ω_0 is correct, the case of $(\Omega_0 = 1, \lambda_0 = 0)$ may lead to the detection of a low frequency harmonic. This is indeed the case. By substituting the word 'lower' for 'higher' in (iii) of the definition of $\mathcal{H}_1$ (Sect. 2.3), and recalculating the equivalent of Fig. 8, the confidence level for rejecting $\mathcal{H}_1(\Omega_0 = 1, \lambda_0 = 0)$ is found to be at the $1 - P > 98\%$ level.

3.2. $\mathcal{H}_2$: what pairs (Ω_0, λ_0) are consistent with the frequency of the peak being at $1/L_{\rm LSS}$?

Given that $\mathcal{H}_1$ is strongly rejected for interesting pairs of (Ω_0, λ_0) values, what are the pairs (Ω_0, λ_0) which are consistent with $L_{\rm LSS} = 130 \pm 10\,h^{-1}$ Mpc?

For consistency, this question is formally answered by trying to reject the null hypothesis $\mathcal{H}_2(\Omega_0, \lambda_0)$, according to which

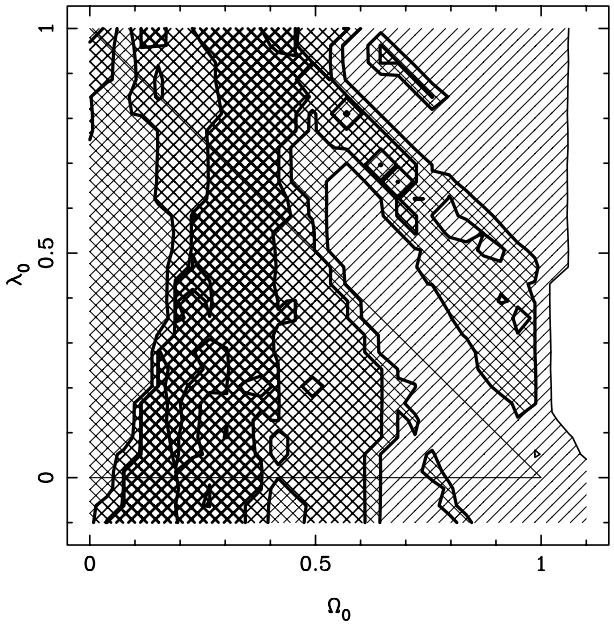

Fig. 8. Combined confidence levels for rejecting $\mathcal{H}_1$, using Eq. (6) to combine the results shown in Fig. 6 and Fig. 7. Shading is as for Fig. 6.

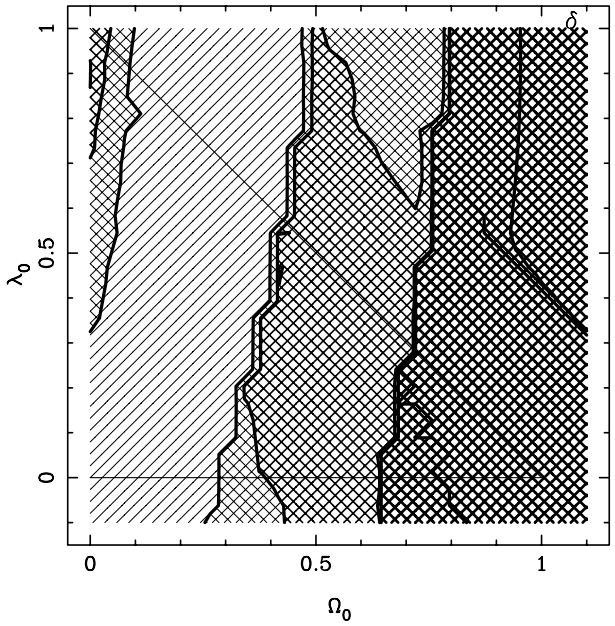

Fig. 10. Confidence intervals for $\mathcal{H}_2$, for the declination subsample, shading as for Fig. 9.

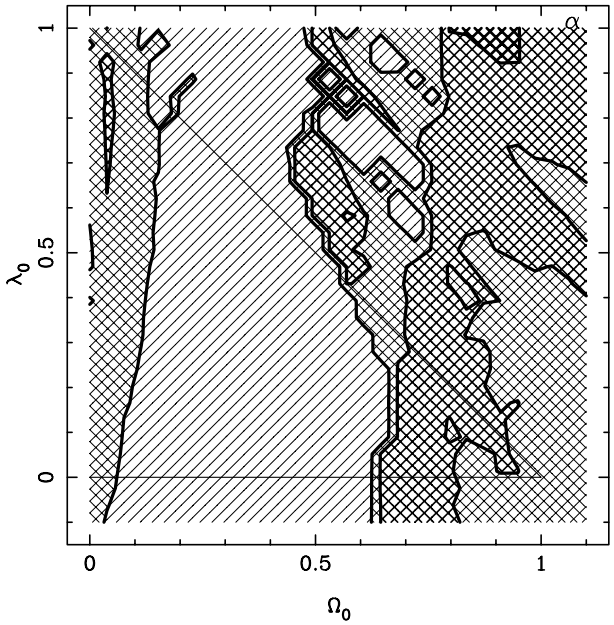

Fig. 9. Confidence intervals for rejecting $\mathcal{H}_2$, the hypothesis that the large scale structure peak occurs at $1/L_{\rm LSS}$, for the right ascension subsample. Shading styles are as for the previous figures, except that the confidence levels are two-sided, i.e. the four successively darker shadings are for $1-P>0\%$, $1-P>68\%$, $1-P>95\%$ and $1-P>99.7\%$ respectively.

the frequency of the peak is assumed to be at $L_{\rm LSS}=130\pm 10\,h^{-1}$ Mpc. Two-sided confidence intervals are used [a factor of two is inserted in front of the integral in Eq. (5)], since the question of interest is now how close the best estimate of the frequency is to the hypothesised frequency, and both low and high frequencies would reject the hypothesis.

The region in the (Ω_0,λ_0) plane for which $\mathcal{H}_2$ cannot be significantly rejected provides an estimate of the values of Ω_0 and λ_0. In the present case, as for most other methods which provide significant constraints on the curvature parameters, there is a degeneracy between the latter, so that an estimate can only be provided for the relation between them, rather than for both parameters independently. A linear fit is used to describe this relation.

Figs. 9 and 10 show the confidence levels for rejecting $\mathcal{H}_2(\Omega_0,\lambda_0)$ for the right ascension and declination subsamples respectively. Neither subsample is sufficient on its own to provide a precise estimate of an (Ω_0,λ_0) relation, although both reject $\Omega_0\gtrsim 0.5$ to $\gtrsim 70\%$ significance.

However, the fact that they are independent subsamples implies that they can be combined via

$$1-P=1-\ P_\alpha[\nu_{\rm max}]\ \ P_\delta[\nu_{\rm max}] \qquad (7)$$

to give Fig. 11, which shows that most values of (Ω_0,λ_0) can be rejected to $>68\%$ confidence if $|\Omega_0-0.25|\gtrsim 0.15$.

More precisely, a linear relation between the two curvature parameters can be fitted to the points in Fig. 11 for which the probability P of obtaining the observations is highest, using the 68% confidence limits as uncertainties, by linear regression of Ω_0 as a function of λ_0.

This relation is

$$\Omega_0=(0.24\pm 0.04)+(0.10\pm 0.08)\,\lambda_0. \qquad (8)$$

The uncertainties here relate to the fitting procedure. Since the $1\,\sigma$ (68% confidence) uncertainties on Ω_0 for each value of λ_0 are not mutually independent, the uncertainties in Eq. 8 do not represent measurement uncertainties.

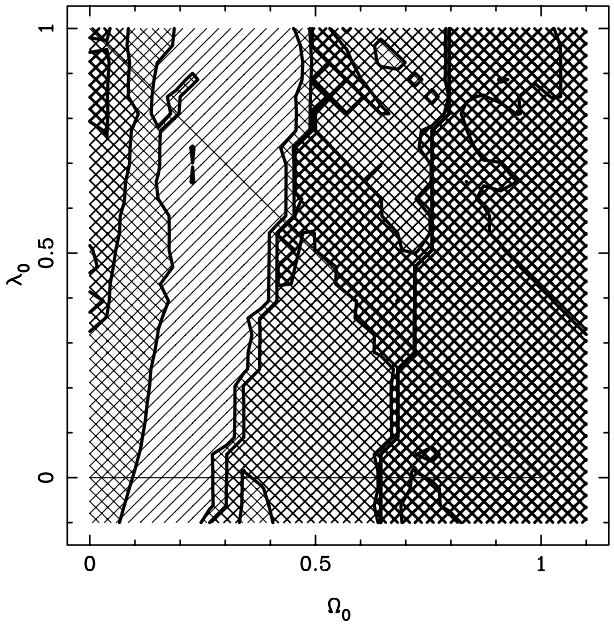

Fig. 11. Confidence intervals for $\mathcal{H}_2$, combining the information from the two subsamples. Shading is as for Fig. 9.

Since the measurement uncertainty (including $\Delta L_{\rm LSS}$) is already expressed in the contours in Fig. 11, this is restored to the zero-point of the relation, giving

$$\Omega_0 = (0.24 \pm 0.15) + (0.10 \pm 0.08)\,\lambda_0, \qquad (9)$$

where the zero-point uncertainty includes known measurement uncertainties and the slope uncertainty relates to the fitting procedure.

Note that, as revealed by this relation, the point least rejected by the data for $\lambda_0 \equiv 0$ is much closer to the large Ω_0 68% confidence limit than to the low Ω_0 68% confidence limit, so the representation by Gaussian uncertainties is not an optimal approximation. However, if one deduces $\Omega_0 = 0.24 \pm 0.15$ for the case $\lambda_0 \equiv 0$ and assumes that this is a Gaussian $1\,\sigma$ uncertainty, then this will be sufficient for most applications, where one prefers overestimates of uncertainties to underestimates.

Alternatively, the $\lambda_0 \equiv 0$ result can be written as $\Omega_0 = 0.24^{+0.05}_{-0.15}$.

For a flat universe, i.e. $\lambda_0 \equiv 1 - \Omega_0$, use of the uncertainties in Eq. (9) as Gaussian uncertainties and combination in quadrature yields $\Omega_0 = 0.30 \pm 0.15$, which is consistent with Fig. 11.

A large part of the uncertainty here is due to the bootstraps. For example, if the intrinsic measurement uncertainty due to the bootstraps is removed, and only the uncertainty $\Delta L_{\rm LSS} = 10\,h^{-1}$ Mpc is used for the equivalent of Fig. 11, then the regions not rejected by the confidence level contours shrink considerably, and $\lambda_0 < 0.4$ is rejected at the $1 - P > 95\%$ level.

However, although bootstrap estimates of uncertainties provide an upper estimate to uncertainties, i.e. the true uncertainties may be smaller, it is prudent to retain the bootstrap estimate.

3.3. Amplitude of large scale structure peak

Since the main aim of the present study is to use the $L_{\rm LSS}$ scale as a ruler for measuring the curvature parameters, a statistically robust estimate of the *amplitude* of the power spectrum peak used as a standard ruler is beyond the scope of this paper.

Indeed, as can be seen in Fig. 6 (upper plot), the amplitude of the peak in the right ascension sub-sample is insufficient (on its own) to significantly rule out the hypothesis of no peak at all, with respect to the Poisson simulations. Of course, the search for a local maximum *does* find that this is closer to ν_0 than expected randomly, for a certain band in the (Ω_0, λ_0) plane.

However, as a guide to what might be expected in future less sparse surveys, the amplitude in the declination subsample, which has a stronger signal than that of the right ascension subsample, may be useful to quantify, though caution is recommended in the interpretation of this estimate.

For the pair $(\Omega_0 = 0.3, \lambda_0 = 0.7)$ (see Sect. 4), a crude estimate of the amplitude expressed as a signal-to-noise ratio,

$$A \equiv \frac{f(\nu_0|\text{obsvn}) - \langle f(\nu_0|\text{Poisson})\rangle}{\langle f(\nu_0|\text{Poisson})\rangle} \pm \frac{\sigma[f(\nu_0|\text{Poisson})]}{\langle f(\nu_0|\text{Poisson})\rangle} \qquad (10)$$

is $A \approx 1.7 \pm 0.5$.

This value is lower than the corresponding value in Broadhurst et al.'s (1990) one-dimensional survey, for which $A \approx 7$ at the $L_{\rm LSS}$ scale (from Fig. 2b of that paper), but is similar in order of magnitude to the density contrast values of $\delta\rho/\rho \gtrsim 2.5$ found in the Las Campanas Redshift Survey (Tucker et al. 1998).

This is not surprising. Even for $(\Omega_0 = 0.3, \lambda_0 = 0.7)$, a somewhat lower amplitude of density contrast can be expected at $z \sim 2$ relative to $z \sim 0$, though this could be compensated for (or under- or over-compensated for) by positive biasing of the quasar distribution relative to that of galaxies, if quasars turn on at the densest points where galaxies are most likely to interact and/or merge.

A full analysis of the amplitude of the signal in analyses following the present one should potentially provide a useful constraint on models of quasar onset and lifetimes.

3.4. Selection effects

The results above are strikingly consistent with the most recent expectations from independent observations regarding large scale structure and the curvature parameters: the power spectrum peak is present at $L_{\rm LSS} = 130 \pm 10\,h^{-1}$ Mpc for the popular curvature pair $(\Omega_0 = 0.3 \pm 0.15, \lambda_0 = 1 - \Omega_0)$.

Could this just be a coincidence due to selection effects? In the redshift direction, selection effects have long led to surprising results, though not to expected results, from quasar catalogues (see Scott 1991 and references therein).

The angular scale corresponding to $z \sim 2$ and $(\Omega_0 \sim 0.3, \lambda_0 = 1 - \Omega_0)$ is $\sim 2°$. This is half an order of magnitude smaller than the size of a UK Schmidt plate ($\approx 6°$). This is sufficiently small that the large scale structure scale is clearly smaller than the size of the plates, but not so much smaller that more subtle effects related to the plate size can be trivially excluded from contributing to the result found above.

Possible angular selection effects, instrumental and/or astrophysical, in objective prism quasar surveys include

(i) effects due to human subjectivity of selecting 'quasar-like' objects from the photographic plates
(ii) not finding quasars in regions where the sky background is noisy or there is no signal at all due to step wedges, large, bright galaxies or to bright stars and their ghosts (due to reflection from the secondary mirror support structure)
(iii) not finding quasars close to other quasars/stars due to overlapping spectra
(iv) differential apparent magnitude limits due to the vignetting function of the telescope plus instrument geometry
(v) differences in apparent magnitude limits between plates
(vi) differential apparent magnitude limits due to intervening dust
(vii) mistaking quasars for stars in low projected number density open (star) clusters which happen to lie in the survey region, thereby missing quasars in those regions
(viii) mistaking stars for quasars, which possibly explains the excess numbers of objects at some specific redshifts in Fig. 5.

Problem (i) is avoided by application of a computer algorithm to digital scans of the Schmidt plates. The validity of the precise quantification and relative weighting of the various 'quasar-like' criteria chosen by Iovino et al. (1996) to detect quasars could be debated, but since they are calculated automatically over the entire scanned regions, this aspect of human subjectivity is applied in a consistent, objective fashion across the plates.

Problems (ii), (iii) to some extent (quasar-star overlaps), (vi), (vii) and (viii) are likely to be minimised by the choice of a very high galactic latitude region, i.e. the SGP.

Problem (v) is corrected for in the control simulations by Poisson distributing points independently within the boundaries of individual plates in each of the two sub-samples (see Sect. 2.2).

The largest obvious contaminants listed in item (ii) which ocur in the fields studied here are a moderately bright star near $\alpha \sim 1^h, \delta \sim -30^\circ$ (field 411, see Table 1 of Iovino et al. 1996) and a bright galaxy near $\alpha \sim 0^h 50^m, \delta \sim 39^\circ$ (field 295), which occupy less than about 0.1 sq. deg. and 0.2 sq. deg. respectively. Neither corresponds to what visually appears to be a void in Fig. 4.

Counting the right ascension and declination analyses separately, the fraction of the solid angle biased by these two objects is $\lesssim [(0.2)+(0.2+0.1)]$ sq. deg./116.4 sq. deg. $= 0.4\%$ of the total solid angle included in the borders (as defined in Table 1). This is unlikely to be sufficient to mimic a large scale structure signal at $\sim 2^\circ$ in the full data set.

Problem (iii) for quasar-quasar overlap could in principle cause a weakening of the real signal and not a false signal, although the low number density of the quasars implies this effect should probably be small. This is because overlaps are expected to occur at around $70''$ in the dispersion direction and $3''$ in the orthogonal direction. If close quasar pairs are missed due to this effect, then the angular distribution measured will be *smoother* than the intrinsic angular distribution, i.e. filamentary type structure would be less easy to detect than it should be.

Quasar-star overlap, and problems (vi), (vii) and (viii) should be uncorrelated with the intrinsic quasar distribution and are more likely to weaken any genuine signal rather than mimic an expected signal.

Table 2. Angular separation of plate centres (Table 1, Iovino et al. 1996) from the four borders [α(1),(2), δ(1),(2) in table, from the borders in strictly increasing numerical α or δ values] and maximum centre-corner angle (3) of the fields for the right ascension (α) and declination (δ) subsamples, defined here in Table 1, in great circle degrees. Field numbers (#) are ESO/SERC field numbers.

	α			δ		
# :	295	296	297	295	351	411
$\alpha(1)$	2.37	2.55	2.53	2.37	1.73	1.40
$\alpha(2)$	2.43	2.45	2.47	1.09	1.97	2.51
$\delta(1)$	2.27	2.26	2.25	2.27	2.77	2.77
$\delta(2)$	2.23	2.24	2.25	2.23	2.23	1.73
(3)	3.33	3.41	3.38	3.29	3.40	3.74

3.4.1. Differential magnitude limits?

Problem (iv) could, in principle, provide the largest systematic error. Fig. 3 of Dawe (1984) shows that from $\approx 2^\circ$ to $\approx 4^\circ$ from the centre of the UK Schmidt Telescope field, the apparent magnitude limit can become less faint from ~ 0.02 mag to ~ 0.2 mag respectively. That is, less quasars would be detectable by a fixed search algorithm towards the edges and corners of the plate than in the middle.

Table 2 lists the angular distances, in great circle degrees, from the boundaries and the corners of the plate images, assuming that the plate centres listed in Table 1 of Iovino et al. (1996) are the correct (B1950) centres of the actual fields observed by those authors.

The borders of the fields, as analysed here (Table 1), are mostly about $2 - 2.5^\circ$ from the centres, so the magnitude limits should vary much less than 0.1 mag over most of the plates. The furthest corners from the centres are mostly at about $3.3 - 3.4^\circ$ from the centres, so the magnitude limit should be about 0.06 mag brighter at these corners.

Are differences in the (solid angular) quasar number densities due to these magnitude limit variations visible in Fig. 4? Possible voids in three of the -42° corners of fields in this figure, and in the $(\alpha = 0^h 42^m, \delta = -37.5^\circ)$ corner of field #351 (the middle declination field) could conceivably be related to the variation in magnitude limit.

However, since the majority of Iovino et al.'s quasars (see Fig. 2 of Iovino et al. 1996) are roughly uniformly distributed over an interval of about one magnitude in apparent magnitude, a change in the magnitude limit of 0.06 mag could at most change the quasar number density by $\sim 6\%$.

Moreover, a small fraction of the quasars in the Iovino et al. sample have $z > 2.4$ and are not studied here. These are likely to have the faintest apparent magnitudes, so $\sim 6\%$ is an

upper estimate to the expected reduction in number density at the furthest corners.

The apparent voids visible to the eye are presumably seen as voids because the number density is at least an order of magnitude lower than average. This is not explicable by a magnitude limit varying by 0.06 mag.

In addition, in at least some of the fields, the number density of quasars appears to be lower in 'voids' near the *centres* of the plates, where the exposure ought to be deepest.

Fig. 4 suggests that the $\delta \sim -30^\circ$ field might appear to have a circularly symmetric central concentration of quasars, apart from a cluster/filament near $(\alpha \sim 0^h42^m, \delta \sim -31^\circ)$. This is partly because the right ascension centres of the declination fields are offset from one another, which is why narrow limits in right ascension were chosen. This could affect an analysis using the boundaries adopted here if that analysis were carried out in right ascension in the 'declination' subsample. But that is not the case here: only the distribution in declination of the declination sample was studied, so the right ascension offsets cannot affect the results.

Another reason why problem (iv) is unlikely to be significant in the present study is that, as Dawe (1984) points out, departures from circular symmetry of the magnitude limit are below the measurement limits (0.01 mag) of his empirical estimates, and are not expected theoretically.

The variations in quasar density *around* the field centres appear about as strong as the variations leading to voids towards field edges or corners. For example, the void centred around $(\alpha = 0^h50^m, \delta = -37^\circ)$ in field #351 (the middle declination field) is adjacent to a quite dense region around $(\alpha = 0^h55^m, \delta = -37^\circ)$, which is about equidistant from the field centre. This strong variation cannot be caused by the circularly symmetric vignetting of the UK Schmidt Telescope.

Finally, shifting several of the borders defined in Table 1 by 0.5° typically modifies the slope and zeropoint of the (Ω_0, λ_0) relation of Eq. (9) by only about ± 0.01. Since magnitude limits should, statistically, have *some* effect at the corners, even if small, this shows that uncertainty due to differential magnitude limits appears to be negligible relative to the basic result.

3.4.2. Selection effects: summary

The possible selection effects discussed above do not seem sufficient to provide a non-cosmological explanation for the present results. It remains that there could be unusual systematic effects not reported by Iovino et al. (1996), e.g. dust on patches of the photographic emulsion, bright supernovae, very bright comet or satellite trails. However, the overall similarity in the results for the right ascension and declination samples makes it unlikely that these could explain the principal results.

3.5. Could the signal be confined to just a small part of the data set?

Although Fig. 5 provides *qualitative* evidence that the signal comes from structures spread through the full data set, it could be possible that this subjective judgment is wrong. Could it be the case that a single structure provides most of the signal, and that very little signal comes from the rest of the full data set?

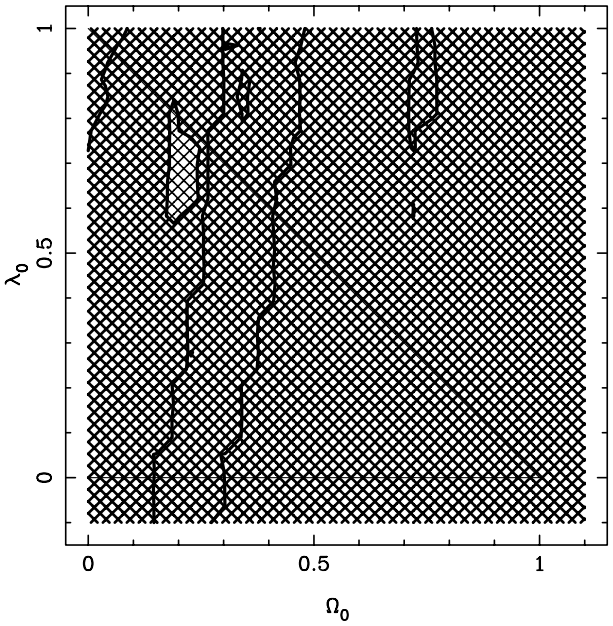

Fig. 12. Confidence intervals from combining Fig. 11 with the relation $0.8\Omega_0 - 0.6\lambda_0 = -0.2 \pm 0.1$ from Perlmutter et al. (1999). Shading is as for Fig. 9.

One possible approach to investigating this is by subdividing the full data set into smaller 'independent' subsets. Given the sparsity of the data set, subdivision into smaller subsets is likely to increase the noise. The $L_{\rm LSS}$ scale has a primarily statistical meaning, and random variation in the estimate of the value of $L_{\rm LSS}$ (something like the standard error in the mean) is likely to be greater in the smaller samples than in the larger samples.

However, in order to provide an illustrative answer to the question, a subdivision of the two subsamples (right ascension and declination) was carried out, into the four redshift intervals $1.8 \leq z < 1.95$, $1.95 \leq z < 2.10$, $2.10 \leq z < 2.25$ and $2.25 \leq z < 2.40$. These provide radial intervals which are close to the $L_{\rm LSS}$ scale, at least for $(\Omega_0 = 0.3, \lambda_0 = 0.7)$. Analyses across the full angular scale were carried out for $\mathcal{H}_1$ and $\mathcal{H}_2$ as before, but dividing the data into eight independent subsamples instead of just two.

The result is that the hypothesis $\mathcal{H}_1(\Omega_0, \lambda_0)$ is rejected more strongly than before, so that the equivalent of Fig. 8 is rejection $1 - P > 98\%$ everywhere in the domain of the (Ω_0, λ_0) plane studied in this paper, and $1 - P > 99.9\%$ over most of this.

This shows that the presence of signals of some sort is stronger in the smaller subsamples than in the larger ones.

However, the length scales at which the signals occur in individual subsamples are noisier in the smaller subsamples, so that if no allowances are made for this, then the final result for $\mathcal{H}_2$, the hypothesis that there is a signal *at the expected scale* $L_{\rm LSS}$ *in every subsample*, is that it is also rejected, to $1 - P > 99.7\%$, for the full range of the (Ω_0, λ_0) plane covered.

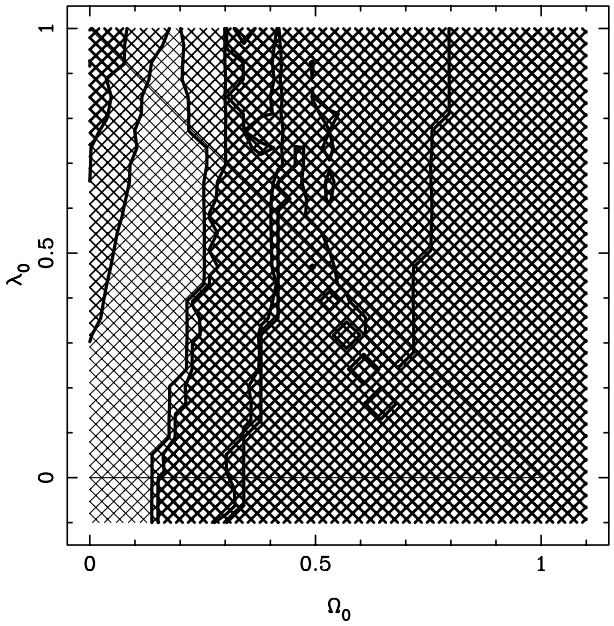

Fig. 13. Confidence intervals for $\mathcal{H}_2$ (cf Fig. 11), for splitting up both of the two subsamples into four redshift subsamples each, and increasing the uncertainty in the power spectrum peak length scale to $\Delta L_{\rm LSS} = 20\,h^{-1}$ Mpc (Sect. 3.5). Shading is as for Fig. 9, i.e. the small patch suggesting a hyperbolic universe model is a $1-P > 95\%$ ('$> 2\sigma$') confidence interval region, and the rest is for $1-P > 99.7\%$.

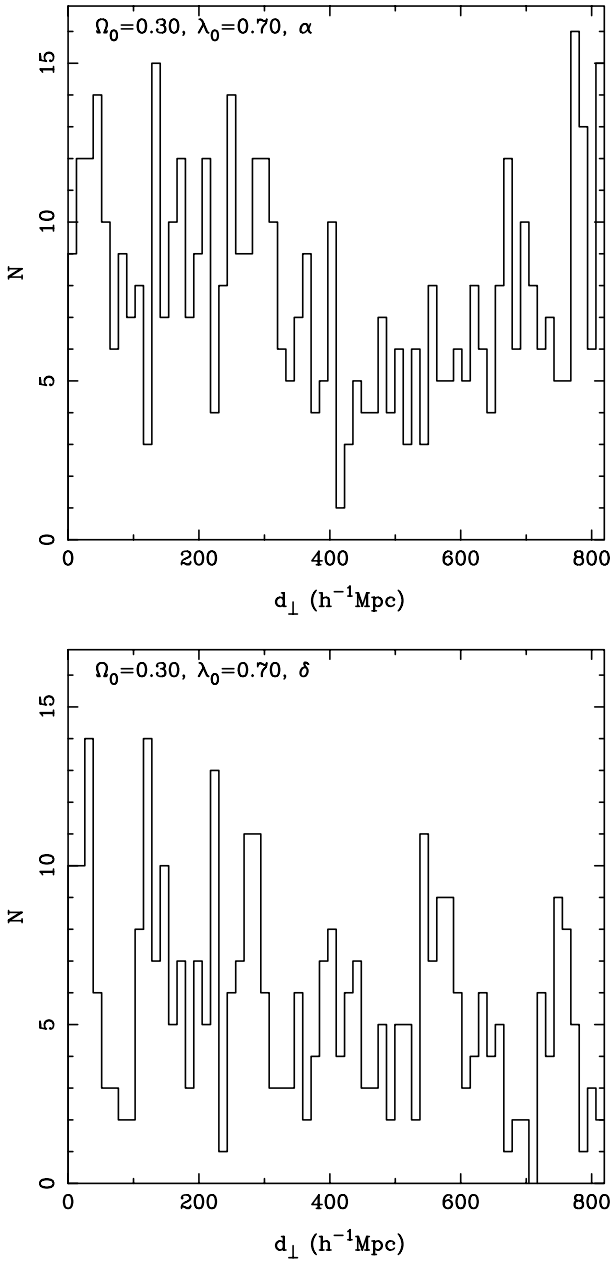

Fig. 14. Confidence intervals for $\mathcal{H}_2$ (cf Fig. 10), for the four redshift subsamples of the declination subsample, retaining $\Delta L_{\rm LSS} = 10\,h^{-1}$ Mpc (Sect. 3.5). Shading is as for Fig. 9, i.e. the lightest shaded region is for the $1-P > 68\%$ confidence interval.

In order to find consistent solutions, either the uncertainty $\Delta L_{\rm LSS}$ needs to be increased, in order to allow for the increased uncertainty per subsample, or some of the subsamples have to be (*a posteriori*) dropped.

Since the number of objects per subsample decreases by roughly a factor of four, a doubling of $\Delta L_{\rm LSS}$ to $\Delta L_{\rm LSS} = 20\,h^{-1}$ Mpc should be sufficient to allow for consistency with the analysis for the full redshift range. This results in a small region which provides a $1-P > 95\%$ solution in a small patch close to the $(\Omega_0 = 0.3, \lambda_0 = 0.7)$ point, but suggesting a hyperbolic universe model (Fig. 13).

Alternatively, retaining $\Delta L_{\rm LSS} = 10\,h^{-1}$ Mpc and just considering the four redshift intervals of the declination subsample leads to Fig. 14. This shows a band in the (Ω_0, λ_0) plane within the $1-P > 68\%$ contour, which is clearly consistent with (though narrower than) the corresponding contour for the declination sample considered as a single sample (Fig. 10).

It is therefore clear that the signal is present in most redshift interval subsets of the full data set, but that because of the increased noise, in order to combine those signals into a consistent solution, a more sophisticated technique than that presented here would be necessary.

4. Discussion and conclusions

It has been shown in this paper that the use of the power spectrum peak corresponding to large scale structure as a standard ruler in the tangential distribution of a homogeneous quasar survey at $z \sim 2$ provides a new and independent method of constraining the curvature parameters.

More precisely, what appears to be the optimal choice of homogeneous tangential quasar surveys publicly available was chosen and analysed. The quasar data analysed were the right ascension and declination subsamples (Table 1) of the Iovino et al. (1996) survey as provided in the Véron-Cetty & Véron (1998) quasar catalogue.

The null hypothesis $\mathcal{H}_1(\Omega_0, \lambda_0)$ according to which no peak can be detected at $L_{\rm LSS} = 130\,h^{-1}$ Mpc in the one-dimensional Fourier transform of the tangential proper motion distance dis-

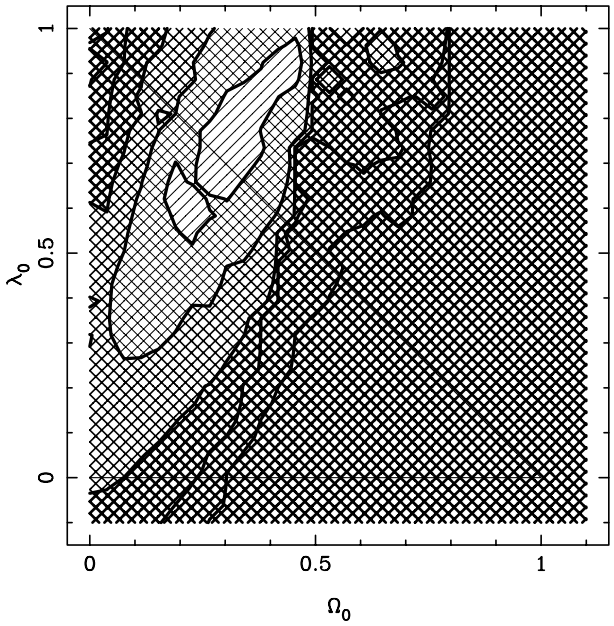

Fig. 15. Tangential length distribution for $(\Omega_0 = 0.3, \lambda_0 = 0.7)$, for the right ascension (upper panel) and declination (lower panel) subsamples (in bins of $12.8\,h^{-1}$ Mpc). The null hypotheses test relate to a power spectrum peak at $L_{\rm LSS} = 130 \pm 10\,h^{-1}$ Mpc. Differences in number density between the plate boundaries are not corrected for, these are corrected for in the simulations.

tributions, and according to which the best estimate of the frequency of any such peak is random, is rejected to high significance for most 'interesting' pairs of (Ω_0, λ_0) in the range $(0.0 \leq \Omega_0 \leq 1.1, -0.1 \leq \lambda_0 \leq 1.0)$. The highest rejection (at a confidence level $1 - P > 99.9\%$) is for a band in the (Ω_0, λ_0) plane running from $\sim (0.15, -0.1)$ to $\sim (0.4, 1.0)$.

Inversion of the frequency condition (iii) of $\mathcal{H}_1(\Omega_0, \lambda_0)$, by replacing 'higher' by 'lower', and recalculating confidence levels results in a rejection of $\mathcal{H}_1(\Omega_0 = 1, \lambda_0 = 0)$ at $1 - P > 98\%$.

Since $\mathcal{H}_1$ is rejected, this implies that a power spectrum peak is present in the data.

Can the power spectrum peak be seen as a 'periodicity' in the data? Fig. 15 allows the reader to judge this subjectively for the pair $(\Omega_0 = 0.3, \lambda_0 = 0.7)$.

Consistently with the points at $(\Omega_0 = 0.3, \lambda_0 = 0.7)$ in the upper panels of Figs. 6 and 7, a periodicity of significant amplitude should be hard to detect in the right ascension sample, but discernable in the declination sample. This is the case in Fig. 15.

Moreover, although the redshift direction is potentially plagued by selection effects, the wedge diagrams in Fig. 5 show clearly that large scale structure can be seen in the $z - \theta$ plane, where $\theta = \alpha \cos\delta$ or $\theta = \delta$ as above. Voids at a scale of around $L_{\rm LSS} \sim 130\,h^{-1}$ Mpc and difficult to explain by selection effects are visible in this figure.

A best estimate for the values of (Ω_0, λ_0) *consistent* with the occurrence of a large scale structure peak in the tangential quasar distribution is found by trying to reject the null hypothesis $\mathcal{H}_2(\Omega_0, \lambda_0)$ according to which the best estimate of the frequency of a peak below $1/d_\perp = 0.01\,h\,{\rm Mpc}^{-1}$ in the Fourier transforms occurs at $1/(L_{\rm LSS} \pm \Delta L_{\rm LSS})$. Bootstraps from the observational data set are used to robustly provide an upper estimate to the observational uncertainty.

Based on a linear fit to the resulting estimates in the (Ω_0, λ_0) plane, the relation $\Omega_0 = (0.24 \pm 0.15) + (0.10 \pm 0.08)\,\lambda_0$ is considered to best summarise the constraints on the two curvature parameters. For zero cosmological constant or flat models, the curvature parameter estimates are $(\Omega_0 = 0.24^{+0.05}_{-0.15}, \lambda_0 \equiv 0)$ and $(\Omega_0 = 0.30 \pm 0.15, \lambda_0 \equiv 1 - \Omega_0)$ respectively.

These estimates of the density parameter are in remarkable agreement with analogous estimates obtained from the kinematics of galaxy clusters (e.g. Carlberg et al. 1997), collapsing galaxy groups (Mamon 1993), as well as from the baryonic fraction in clusters (White et al. 1993; Mohr et al. 1999) and groups (Henriksen & Mamon 1994).

The estimate of the cosmological constant under the assumption of a flat model is also remarkably close to those which now tend towards a flat, cosmological constant dominated universe from faint galaxy number counts, the galaxy depletion curve behind clusters, the supernovae type Ia method (Fukugita et al. 1990; Fort et al. 1997; Chiba & Yoshii 1997; Perlmutter et al. 1999; Riess et al. 1998) and cosmic microwave background methods. Results from the latter are being updated rapidly at the moment, and are dependent on numerous assumptions which do not enter either the present method or the supernovae type Ia method, so are not discussed here.

The present method is very independent of the supernovae type Ia method: in choice of astrophysical object, in the redshift range and in the difference between using standard candles versus standard rulers. What is the result of combining the two?

The combination of the present result with the relation $0.8\,\Omega_0 + 0.6\,\lambda_0 = -0.2 \pm 0.1$ from Perlmutter et al. (1999), where the error is modelled as Gaussian, results in Fig. 12.

Although the two relations are not quite orthogonal, they have different enough slopes that the uncertainty in both is considerably reduced, such that a nearly flat model is implied *without using any cosmic microwave background* information.

A linear fit to the 68% confidence contour in Fig. 12, for Ω_0 as a function of $(\lambda_0 - 0.7)$, results in:

$$\Omega_0 = (0.30 \pm 0.02) + (0.57 \pm 0.11)(\lambda_0 - 0.7), \quad 0.55 < \lambda_0 < 0.95, \tag{11}$$

where as before, the uncertainties from linear regression relate to the fitting procedure and underestimate the true uncertainties shown in the figure.

In this case, the maximum uncertainty in Ω_0 for a given value of λ_0 in the range above is $\sigma(\Omega_0) = 0.11$. Restoring this to the relation as before yields:

$$\Omega_0 = (0.30 \pm 0.11) + (0.57 \pm 0.11)(\lambda_0 - 0.7), \quad 0.55 < \lambda_0 < 0.95. \tag{12}$$

This combined result strongly supports the possibility that the observable universe satisifies a nearly flat, perturbed

Friedmann-Lemaître-Robertson-Walker model, where 'nearly' is quantified as ± 0.1 in the two dimensionless curvature parameters. It does not require prior assumptions on the cosmological constant, nor does it use cosmic microwave background (CMB) data.

An independent confirmation that no systematic errors are present in the data studied here (or else an independent estimate of the systematic errors) would obviously be very desirable.

If further observations confirm that large scale structure can be used as a standard ruler, then surveys such as the 2dF (2 degree field) and SDSS (Sloan Digitial Sky Survey) quasar surveys should provide confirmation of the present results within the next few years.

The former risks systematic error from the fact that the angular scale corresponding to $L_{\rm LSS} = 130 \pm 10\,h^{-1}$ Mpc at $z \sim 2$ is 2°: this is the field size of the 2dF survey. Careful correction for this, use of lower redshift quasars, and a much higher signal-to-noise ratio would help in obtaining convincing results from the former. However, since the SDSS is digital, it should presumably avoid this problem.

The present method would be ideally suited to a deep right ascension survey (i.e. for a narrow band in declination but a long, e.g. 60°, band in right ascension), which avoids any risk of dependence of any angular scale near a few degrees but includes a fair sample of quasars at $z \sim 2$, sampling a few hundred quasars per great circle degree. A blind, deep, slit spectroscopic, right ascension survey, 'blind' in the sense of taking spectra of *all* objects in a very narrow declination interval, would provide possibly one of the fastest ways of obtaining constraints in the (Ω_0, λ_0) plane which should suffer little from possible selection effects. This offers a valuable cosmological project for the planned liquid mercury LZT (Large Zenith Telescope).

Another survey to which the present method could be usefully applied will be the combined VIRMOS (Visual and Infrared MultiObject Spectroscopy, on the VLT) and XMM (X-ray Multiple Mission, X-ray satellite) survey, which should trace out the filaments and/or walls of several units of large scale structure at super-unity redshifts via several different astrophysical tracers: galaxies, quasars and hot gas.

Over the next few years, if the precision in the present application of this method were increased by an order of magnitude in the new quasar surveys, then, together with more confidence in understanding systematic errors in the supernovae type Ia method and reduction in random errors by more detections at high redshifts, that would imply estimates on Ω_0 and on λ_0 to a precision of ± 0.01 — again without use of CMB data.

Interest may then shift to the other geometrical parameters: those required to determine the size of the Universe. As pointed out by Schwarzschild (1900, 1998), both the curvature and the topology of space need to be known in order to know the size of the Universe. For background and recent reviews on progress in observational methods for measuring the topological parameters, see Lachièze-Rey & Luminet (1995), Starkman (1998; and following papers in that volume), Luminet (1999) and Luminet & Roukema (1999). Moreover, a side effect of a significant measurement of the global geometry of the Universe would be a confirmation or refinement of the estimates of the local geometrical parameters (Roukema & Luminet 1999).

Acknowledgements. We thank Stéphane Colombi, Emmanuel Bertin, Guy Mathez, Bernard Fort, Enrique Gaztañaga, Jasjeet Bagla, Shiv Sethi, Daniel Kunth, Steve Hatton and an anonymous referee for useful comments. Use of the resources at the Centre de Données astronomiques de Strasbourg (*http://csdweb.u-strasbg.fr*), the support of the Institut d'astrophysique de Paris, CNRS, for a visit during which part of this work was carried out, and the support of la Société de Secours des Amis des Sciences are gratefully acknowledged.

References

Adelberger K.L., Steidel C.C., Giavalisco M., et al., 1998, ApJ 508, 18
Barrow J.D., Sonoda D.H., Bhavsar S.P., 1984, MNRAS 210, 19P
Baugh C.M., Efstathiou G., 1993, MNRAS 265, 145
Baugh C.M., Efstathiou G., 1994, MNRAS 267, 323
Broadhurst T., 1999, In: Le Brun V., Mazure A., Le Fèvre O. (eds.) Clustering at High Redshift. in press
Broadhurst T.J., Ellis R. S., Koo D.C., Szalay A.S., 1990, Nat 343, 726
Broadhurst T., Jaffe A.H., 1999, submitted (arXiv:astro-ph/9904348)
Carlberg R.G., Yee H.K.C., Ellingson E., 1997, ApJ 478, 462
Chiba M., Yoshii Y., 1997, ApJ 489, 485
da Costa L.N., 1992, In: Mamon G.A., Gerbal D. (eds.) 2nd DAEC Meeting, The Distribution of Matter in the Universe. Obs. de Paris, Meudon, p. 163, ftp://ftp.iap.fr/pub/from_users/gam/PAPERS/DAECMTG/dacosta.dvi.Z
da Costa L.N., 1993, In: Bouchet F., Lachièze-Rey M. (eds.) 9th IAP Astrophysics Meeting, Cosmic Velocity Fields. Editions Frontières, Gif-sur-Yvette, France, p. 475
Dawe J.A., 1984, In: Capaccioli M. (ed.) IAU Coll. 78, Astronomy with Schmidt-type Telescopes. Reidel, Dordrecht, p. 193
de Lapparent V., Geller M.J., Huchra J.P., 1986, ApJ 302, L1
Deng Z., Xiaoyang X., Fang L.-Zh., 1994, ApJ 431, 506
Deng X.-F., Deng Z.-G., Xia X.-Y., 1996, Chin. Astron. Astroph. 20, 383
Einasto M., Einasto J., Tago E., Dalton G. B., Andernach H., 1994, MNRAS 269, 301
Einasto J., Einasto M., Frisch P., et al., 1997a, MNRAS 289, 801
Einasto J., Einasto M., Gottlöber S., et al., 1997b, Nat 385, 139
Fort B., Mellier Y., Dantel-Fort M., 1997, A&A 321, 353
Fukugita M., Yamashita K., Takahara F., Yoshii Y., 1990, ApJ 361, L1
Gaztañaga E., Baugh C.M., 1998, MNRAS 294, 229
Geller M.J., Huchra J.P., 1989, Sci 246, 897
Giavalisco M., Steidel C.C., Adelberger K.L., et al., 1998, ApJ 503, 543 (arXiv:astro-ph/9802318)
Guzzo L., 1999, In: Proceedings of XIX Texas Symp. Rel. Astr. (arXiv:astro-ph/9911115)
Iovino A., Clowes R., Shaver P., 1996, A&AS 119, 265
Hartwick F.D.A., Schade D., 1990, ARA&A 28, 437
Henriksen M.J., Mamon G.A., 1994, ApJ 421, L63
Lachièze-Rey M., Luminet J.-P., 1995, Phys. Rep. 254, 136 (arXiv:gr-qc/9605010)
Luminet J.-P., 1999, In: Concepts de l'Espace en Physique. Les Houches, 29 sep - 3 oct 1997, Acta Cosmologica 24, (arXiv:gr-qc/9804006)
Luminet J.-P., Roukema B.F., 1999, In: Lachièze-Rey M. (ed.) Theoretical and Observational Cosmology. NATO Advanced Study In-

stitute, Cargèse 1998, Kluwer, Netherlands, p. 117 (arXiv:astro-ph/9901364)
Mamon G.A., 1993, In: Combes F., Athanassoula E. (eds.) The N-Body Problem & Gravitational Dynamics. Obs. Paris, Meudon, p. 188, (arXiv:astro-ph/9308032)
Mohr J.J., Mathiesen B., Evrard A.E., 1999, ApJ 517, 627
Perlmutter S., Alderling G., Goldhaber G., et al., 1999, ApJ 517, 565 (arXiv:astro-ph/9812133)
Riess A.G., Fillippenko A.V., Challis P., et al., 1998, AJ 116, 1009
Roukema B.F., Luminet J.-P., 1999, A&A 348, 8 (arXiv:astro-ph/9903453)
Schwarzschild K., 1900, Vier. d. Astr. Gess. 35, 337
Schwarzschild K., 1998, ClassQuantGra 15, 2539 [English translation of Schwarzschild (1900)]
Scott D., 1991, A&A 242, 1
Starkman G.D., 1998, ClassQuantGra 15, 2529
Tucker D.L., Lin H., Shectman S., 1998, In: Colombi S., Mellier Y., Raban B. (eds.) XIVth IAP Astrophysics Meeting, Wide Field Surveys in Cosmology
Véron-Cetty M.P., Véron P., 1998, ESO Scientific Report 18, http://cdsweb.u-strasbg.fr/viz-bin/VizieR?-source=VII/207/
Weinberg S., 1972, Gravitation and Cosmology. Wiley, New York, USA
White S.D.M., Navarro J.S., Evrard A.E., Frenk C.S., 1993, Nat 366, 429